Nanocrystallization induced by quasi-static fracture of metallic glasses at room temperature

J. T. Fan [a]; Z. F. Zhang [a]; S. X. Mao [b]; B. L. Shen [cd]; A. Inoue [d]

[a] Shenyang National Laboratory for Materials Science, Institute of Metal Research, Chinese Academy of Science, Shenyang, P.R. China [b] Department of Mechanical Engineering, University of Pittsburgh, Pittsburgh, PA, USA [c] Ningbo Institute of Materials Technology and Engineering, Chinese Academy of Sciences, Ningbo, P.R. China [d] Institute for Materials Research, Tohoku University, Sendai, Japan

Online Publication Date: 01 November 2008

PLEASE SCROLL DOWN FOR ARTICLE

Taylor & Francis
Taylor & Francis Group

Nanocrystallization induced by quasi-static fracture of metallic glasses at room temperature

J.T. Fan[a]*, Z.F. Zhang[a]*, S.X. Mao[b], B.L. Shen[cd] and A. Inoue[d]

[a]*Shenyang National Laboratory for Materials Science, Institute of Metal Research, Chinese Academy of Science, Shenyang, P.R. China;* [b]*Department of Mechanical Engineering, University of Pittsburgh, Pittsburgh, PA, USA;* [c]*Ningbo Institute of Materials Technology and Engineering, Chinese Academy of Sciences, Ningbo, P.R. China;* [d]*Institute for Materials Research, Tohoku University, Sendai, Japan*

Nanoparticles on the fracture surfaces of Co- and Fe-based metallic glasses during quasi-static compression at room temperature have been observed using a high-resolution scanning electron microscope. In terms of the differential scanning calorimeter, those nanoparticles were identified to be a result of nanocrystallization induced by the rapid fracture. Finally, the nanocrystallization behavior was evaluated by taking into account the super-high crack propagation rate and high elastic energy, which contributed to the local temperature rise up to the onset of crystallization, T_x.

Keywords: metallic glass; nanocrystallization; fracture; room temperature

1. Introduction

Recently, the mechanical properties of Bulk Metallic Glasses (BMGs) have become a hot topic of scientific and technological interest, owing to their exceptional high strength and elastic limit [1–3]. As is well known, BMGs are disordered over long-range scales and have no crystallographic planes for slip deformation. Thus, under appropriately high stress levels and at temperatures below the glass-transition temperature, T_g, inhomogeneous plastic deformation always occurs and is characterized by the localization of plastic strain in narrow shear bands [4,5]. Usually, it may be assumed that localized adiabatic heating occurs within a shear band or shear plane. Also the large amount of energy often dissipates within a narrow shear band at a very fast rate, leading to an instability followed by catastrophic failure. Many experimental results have been reported concerning the temperature rise, ranging from 400 to 3175 K for various BMGs [6]. Calculations from the elastic energy transformation result in a temperature rise from 0.05 to 2500 K [7]. Some other reports showed compelling evidence to a temperature rise in the vicinity of shear bands and adiabatic heating during fracture [8,9]. In addition, nanocrystallization behavior has been discussed for some BMGs under various conditions, for example: nanoindentation at room temperature [7], bending of thin ribbons [10], high-energy

---

*Corresponding authors. Email: jtfan@imr.ac.cn; zhfzhang@imr.ac.cn

ball milling, mechanical alloying, and thermal annealing [11,12]. However, no reliable experimental evidence is available to elucidate the mechanisms of deformation-induced crystallization in an amorphous alloy under well-controlled and slow quasi-static compressive tests. In this letter, we report observations on nanoparticles on the fracture surfaces of Co- and Fe-based BMGs, induced by uniaxial compressive testing at room temperature, using a high-resolution LEO SUPER35 Scanning Electron Microscope (SEM) with a resolution of 1.5 nm. In addition, we applied Differential Scanning Calorimetry (DSC) to show that the nanoparticles originated from nanocrystallization during rapid fracture.

2. Experimental procedures

Multicomponent Co- and Fe-based alloy ingots with nominal compositions of $Co_{43}Fe_{20}Ta_{5.5}B_{31.5}$ and $Fe_{65.5}Cr_4Mo_4Ga_4P_{12}C_5B_{5.5}$ (at.%) were prepared by arc-melting the mixtures and ejection copper mold casting in a Ti-gettered highly pure argon atmosphere. Details of the preparation methods have been reported before [13,14]. X-ray Diffraction (XRD) shows that there is only a series of broad diffraction maxima without any detectable sharp Bragg peaks, indicating a fully amorphous glass structure. The compression samples, with diameter of 2 mm and height of 4 mm, were cut from the as-cast BMG rods, and then carefully machined and polished. Three samples were tested and the averaged results were used. The compression tests were carried out on a computed-controlled, servo-hydraulic Instron-8810 testing machine with a strain rate of about $10^{-4}\,s^{-1}$ at room temperature. The compression strain was measured by a strain-gauge meter with a high accuracy. Finally, the fracture surfaces were observed using a high-resolution LEO SUPER35 SEM with a resolution of 1.5 nm. Meanwhile, the as-cast and fractured samples for the Co- and Fe-based BMGs were studied in a Perkin–Elmer differential scanning calorimeter (DSC-7) under the flowing purified argon gas at a heating rate of 1 K/s to reveal the crystallization behavior.

3. Results and discussion

Figure 1 shows the quasi-static compressive engineering stress–strain curves of the Fe- and Co-based BMG samples. For the Fe-based BMG sample, the stress–strain curve is linear up to an elastic strain of about 2.3%, with a super-high fracture strength, $\sigma_{c,f}$ of 4480 MPa without distinct plastic deformation; this is higher than that of another Fe-based metallic glasses [15]. However, there is still a yield behavior with a strength $\sigma_{c,y}$ of about 4350 MPa. The same is the case for the Co-based BMG sample, which also exhibits a super-high fracture strength, $\sigma_{c,f}$ of 4980 MPa. The strength is slightly lower than that in Ref. [13], maybe due to differences in strain rate or experimental error [16,17]. The elastic deformation is linear up to a strain of about 2.2%, followed by a slight yield behavior with a strength $\sigma_{c,y}$ of about 3950 MPa. There is also no notable plastic deformation.

   Dynamic fracture was found in certain metallic glasses [18,19]. Some researchers concluded that the fracture of brittle material always occurs at a very high velocity, about 0.7–$0.9\upsilon_R$, with a dynamic instability (here υ_R is the Rayleigh wave velocity, about 4.5 km/s) [20–22]. The current Fe- and Co-based BMG samples are very brittle and display a fragment fracture, as in the previous observations [17,19]. In general, the dynamic crack
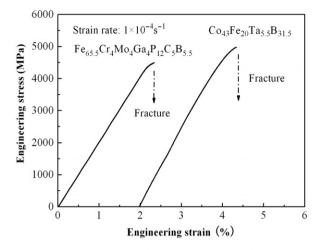
Figure 1. Engineering stress–strain curves of Co- and Fe-based metallic glasses, subjected to a uniaxial compressive test with a constant strain rate of $1 \times 10^{-4}\,\mathrm{s}^{-1}$ at room temperature.

propagation velocity can reach a high value with a wavy cleavage fracture [17]. In order to conservatively estimate the fracture processes, we assume that the crack propagation velocity is only $0.1\upsilon_R$ (about $450\,\mathrm{m/s}$) for the current Fe- and Co-based BMGs. Thus, the time for the crack to go through the longest distance of the current sample (about 4 mm) is about $9 \times 10^{-6}\,\mathrm{s}$. Such a short time is insufficient to allow rapid diffusion of the high elastic energy. It is considered that there is a static elastic energy density, $G_S = \sigma_S^2/2E_S$ ahead of the crack tip (where E_S is the static elastic modulus and σ_S is the static fracture strength) [19]. So, the static elastic energy densities were calculated to be about 50 and 54 $\mathrm{MJ\,m^{-3}}$ for the Fe- and Co-based BMGs, respectively. During the fracture, the dynamic energy density in the tip of crack, $G_D = \sigma_D^2/2E_D$, was considered to be greater than the static elastic energy density [19]. Thus, much excess elastic energy cannot diffuse outside in such a limited time, and only dissipates within a narrow band, leading to adiabatic heating with a great temperature rise and contributing to the formation of adiabatic shear bands.

Figure 2 shows SEM images of the Co-based BMGs after failure under uniaxial compressive test at room temperature. One shear band was observed on the surface, together with some cracks (Figure 2a), implying a local shear deformation behavior, which corresponds to the slight yielding phenomena in the stress–strain curve. On the fracture surface, a vein pattern can be seen locally during the fast fracture, similar to that in Zr-based BMGs [23]. Furthermore, the coexistence of the bugle-like patterns and nanoparticles can be clearly seen within a close neighbourhood, as shown in regions I and II (Figure 2b). The magnified photograph of region I clearly displays the bugle-like patterns along with the elongated viscous liquid. Their length is about $2\,\mu\mathrm{m}$ (Figure 2c), resulting from the local shear plastic flow, corresponding to the shear bands on the surface (Figure 2a). The viscous liquid implies a local softening behavior, due to the temperature rise. Under the shear stress, the viscous liquid becomes elongated along the shear stress direction. In addition, the amplified photograph of region II, close to region I, shows crystallized particles on the nanoscale, covered by the melted liquid (Figure 2c). The particle size is from 10 to 100 nm, and hence designated as nanocrystals. From the discussion above, since the regions I and II are very close, they should have the same
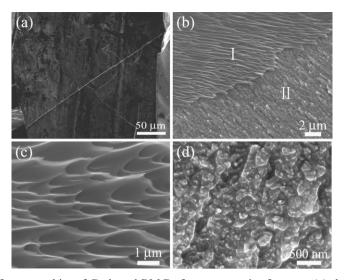
Figure 2. SEM fractographies of Co-based BMG after compressive fracture. (a) shear bands on the surface; (b) melted vein-like structure together with some nanoparticles; (c) amplified vein-like structure with the same shear direction in region I; (d) magnified nanoparticles in region II.

temperature rise during rapid fracture. Much viscous liquid was found in region I, which implies the temperature rise surpasses the crystallization temperature, T_x. In addition, much liquid, overlaying on the nanoparticles, indicates a high temperature rise in regions II. Therefore, it is reasonable to conclude that the nanoparticles result from the crystallization behavior of the amorphous alloy under uniaxial compressive test at room temperature, due to the adiabatic heating in a local narrow band.

In addition, for the Fe-based BMG sample, a similar phenomenon was also found on the fracture surfaces, after uniaxial compressive test at room temperature. Figure 3a shows bugle-like patterns and nanoparticles, in close neighborhood, designated as regions I and II, respectively. The amplified photograph shows many nanoparticles with sizes from 20 to 150 nm (Figure 3b). Furthermore, a crack was observed across the nanoparticles, as indicated by the arrow. The amplified photograph of the bugle-like patterns shows the elongated viscous liquid about 4 μm in length (Figure 3c). Further observation shows that in the core of the bugle-like patterns, there are also some nanoparticles, as indicated by the circle in Figure 3d, which further confirm the occurrence of nanocrystallization under the compressive test at room temperature. Therefore, although the Fe-based BMG generally has a high glass-forming ability (GFA) [24], crystallization happened during fracture.

In order to confirm the nanocrystallization referred to above, the fractured Co-based samples were collected and studied in the Perkin–Elmer differential scanning calorimeter (DSC-7), as well as the as-cast sample for comparison (Figure 4). For the as-cast sample, ensured as fully amorphous structure by XRD, the glass transition appears as a change in heat capacity at T_g (901 K). This is followed by a series of exothermic peaks, which begin at the onset of crystallization, T_x (966 K). With further heating, the sample began to melt at the solidus temperature, T_s (1450 K), and then completely melted at the liquidus temperature, T_l (1562 K). The crystalline and glassy states have equivalent Gibbs free-energy at the fusion temperature, T_f, which was estimated by using the melting
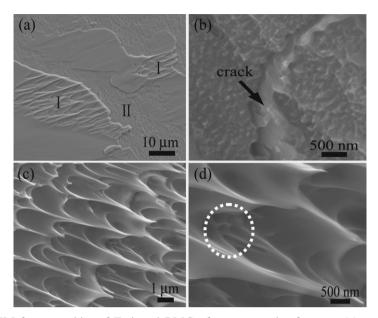
Figure 3. SEM fractographies of Fe-based BMG after compressive fracture. (a) melted vein-like structure together with some nanoparticles; (b) magnified nanocrystalline phases together with a crack; (c) vein-like structure with the same direction in region I; (d) magnified vein-like structure with some nanoparticles inside.
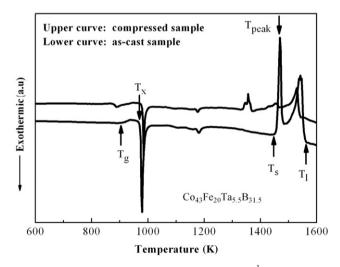

Figure 4. DSC traces of Co-based BMG at a heating rate of $1 \, K \, s^{-1}$ for the fractured sample and the as-cast sample in compression.

peak temperature. By integrating the area of the melting event, the total heat of fusion, ΔH_f was calculated to be about 12.8 kJ/g atom. The entropy of fusion can then be estimated as $\Delta S_f = \Delta H_f / T_f$. With a melting peak temperature of 1470 K, ΔS_f was calculated as 8.71 J/g atom K. This value of ΔS_f is an important consequence on the

driving force for crystallization and the solid–liquid interfacial energy. Besides, for the fractured sample, the exothermic peak dives down sharply compared with the as-cast sample, indicating the occurrence of crystallization under the uniaxial compressive test at room temperature. Furthermore, the solidus temperature, T_s (about 1334 K) becomes smaller than that of the as-cast alloy (about 1450 K). That indicates the fractured sample is easier to melt than the as-cast sample, which can be attributed to the previously formed nanocrystals in the fractured sample. Besides, the melting heat of the fractured sample declines more compared to that of the as-cast sample, which also implies the pre-formation of nanocrystals during compressive test.

Finally, it is in principle possible for the total formation of nanocrystals during compressive test. The amorphous alloys are in thermodynamically metastable states and will transfer into the stable states under appropriate circumstances. The driving force for the crystallization is the difference in the Gibbs free energies between the amorphous and the crystalline states, $\Delta G^{n-a}(T)$, given in the following equations: $\Delta G^{n-a}(T_X) = \Delta H^{n-a}(T_X) - T_X \Delta S^{n-a}(T_X)$ [12]. $\Delta H^{n-a}(T_X)$ is the difference in the enthalpies between the amorphous and nanocrystalline states at the crystallization temperature, T_X. $\Delta S^{n-a}(T_X)$ is the difference in the entropies between the amorphous and nanocrystalline states at the temperature, T_X. Generally, when the temperature is as high as T_X, because the difference in the Gibbs free energies $\Delta G^{n-a}(T)$ is less than zero, the amorphous state will spontaneously transform to the crystal. To explain such a high mobility of atoms, several possibilities are considered here. A large local temperature rise, up to several hundreds of degrees, has also been suggested to result from the adiabatic shearing of metallic glass [25]. Such a situation may be more likely during dynamic loading and/or fracture with a high crack propagation rate. For the present situation of shear bands connected to a super-high fracture rate, an estimated adiabatic temperature rise, ΔT inside a shear band should be $\Delta T = (\beta/\rho C_P) \int_0^{\varepsilon_f} \sigma \mathrm{d}\varepsilon$. Here, β is the fraction of elastic work converted into heat; ρ is the density (about 7.86 g cm^{-3} for Co-based BMG); C_P is the specific heat (roughly equal to 0.55 J gk^{-1} for a typical metallic glass [26]); σ is the flow stress; and ε_f is the final strain. In order to conservatively estimate, we assume that the value of β is equal to 0.1 (assumed to be 0.9 for crystalline Fe [27]). Therefore, the estimated adiabatic temperature rise, ΔT inside a shear band should be 1480 K, which is more than the onset of crystallization, T_x (equal to 966 K). Therefore, in principle, this case meets the thermodynamic condition for crystallization.

4. Conclusions

There exist nanoscale particles on the fracture surface of Co- and Fe-based BMG samples during quasi-static compression at room temperature. Based on DSC data and the thermal analysis, it is suggested that the nanocrystallization behavior should occur in some local regions on the fracture surface of the brittle Fe- and Co-based BMG samples during quasi-static compression at room temperature. The super-high crack propagation rate and the high elastic energy might contribute to the large temperature rise, up to the onset of crystallization temperature T_x. The current results provide a new understanding on the fracture behavior of the brittle Co- and Fe-based amorphous alloys, together with a new view to the nanocrystallization.

Acknowledgments

References

[1] W.J. Wright, R. Saha and W.D. Nix, Mater. Trans. 42 (2001) p.642.
[2] J.G. Wang, B.W. Choi, T.G. Nieh et al., J. Mater. Res. 15 (2000) p.798.
[3] A. Inoue, Acta Mater. 48 (2000) p.279.
[4] P.E. Donovan, Acta Mater. 37 (1989) p.445.
[5] Z.F. Zhang, F.F. Wu, G. He et al., J. Mater. Sci. Tech. 23 (2007) p.747.
[6] B. Yang, M.L. Morrison, P.K. Liaw et al., Appl. Phys. Lett. 86 (2005) p.141904.
[7] J.J. Kim, Y. Choi, S. Suresh et al., Science 295 (2002) p.654.
[8] J.J. Lewandowski and A.L. Greer, Nat. Mater. 5 (2006) p.15.
[9] M.H. Lee and D.J. Sordelet, Appl. Phys. Lett. 88 (2006) p.261902.
[10] H. Chen, Y. He, G.J. Shiflet et al., Nature 367 (1994) p.541.
[11] Y. He, G.J. Shiflet and S.J. Poon, Acta Metall. Mater. 43 (1995) p.83.
[12] K. Lu, Mater. Sci. Eng. R 16 (1996) p.161.
[13] A. Inoue, B.L. Shen, H. Koshiba et al., Acta Mater. 52 (2004) p.1631.
[14] M. Stoica, J. Eckert, S. Roth et al., J. Alloy Compd. 434 (2007) p.171.
[15] Q.J. Chen, J. Shen, D.L. Zhang et al., J. Mater. Res. 22 (2007) p.358.
[16] G. Wang, D.M. Chen, J. Shen et al., J. Non-Crys. Solids 352 (2006) p.3872.
[17] Z.F. Zhang, H. Zhang, B.L. Shen et al., Philos. Mag. Lett. 86 (2006) p.643.
[18] J. Shen, W.Z. Liang and J.F. Sun, Appl. Phys. Lett. 89 (2006) p.121908.
[19] Z.F. Zhang, F.F. Wu, W. Gao et al., Appl. Phys. Lett. 89 (2006) p.251917.
[20] M.J. Buehler and H.J. Gao, Nature 439 (2006) p.307.
[21] E. Sharon, S.P. Gross and J. Fineberg, Phys. Rev. Lett. 76 (1996) p.2117.
[22] T. Cramer, A. Wanner and P. Gumbsch, Z. Metallkd. 90 (1999) p.675.
[23] J.T. Fan, F.F. Wu, Z.F. Zhang et al., J. Non-Cryst. Solids 353 (2007) p.4707.
[24] J. Shen, Q.J. Chen, J.F. Sun et al., Appl. Phys. Lett. 86 (2005) p.151907.
[25] H.J. Leamy, H.S. Chen and T.T. Wang, Metall. Trans. 3 (1972) p.699.
[26] A.S. Argon, Acta Metall. 27 (1979) p.47.
[27] Y. Bai and B. Dodd, *Adiabatic Shear Localization*, Pergamon Press, New York, 1992.